# Occupational Exposure to Hazardous Airborne Pollutants: Effects of Air Mixing and Source Location

## Donghyun Rim & Atila Novoselac

# Occupational Exposure to Hazardous Airborne Pollutants: Effects of Air Mixing and Source Location

## Donghyun Rim and Atila Novoselac

Department of Civil, Architectural and Environmental Engineering, University of Texas at Austin,
Austin, Texas

*The presence of airborne pollutants in indoor environments has been associated with occupants' discomfort and/or adverse health effects. This study investigates occupational exposure in relation to indoor air mixing and source location relative to a human body. Experimental and computational methods were used to provide information about the pollutant distribution in the vicinity of the human body for different levels of room air mixing. Study results show that the often used assumption of uniform pollutant distribution in an occupied space is not always appropriate for estimation of inhalation exposure. Results also indicate that an occupant may experience very high acute exposure to airborne pollutants when little air mixing exists in a space and the pollutant source is in the vicinity of the occupant. The buoyancy-driven flow induced by the convective heat transfer from an occupant's body can transport pollutants in the occupant's vicinity to the breathing zone. Specific study results reveal that a source located in the occupant's front chest region makes a relatively large contribution to the breathing zone concentration compared with the other sources in the vicinity of the human body. With the source position in this region, exposure can be nine times greater than that calculated with the uniform mixing assumption. The buoyancy-driven convective plume around a body seems to have a significant influence on pollutant transport and human exposure, especially in the absence of room air mixing.*

**Keywords** air mixing, airborne pollutants, CFD, occupational exposure, source location

Address correspondence to: Donghyun Rim, Department of Civil, Architectural and Environmental Engineering, ECJ 5.422, University of Texas at Austin, 1 University Station C1752, Austin, TX 78712-1076; e-mail: mcdhrim@gmail.com.

## INTRODUCTION

Inhalation exposure to indoor airborne pollutants has been associated with occupant comfort and adverse health problems.[1–4] Many occupational respiratory diseases are caused by exposure to hazardous aerosol and gaseous pollutants.[4–6] For instance, occupational asthma, which is caused by acute brief exposure to airborne contaminants, has been implicated in 9 to 15% of adult asthma cases.[7]

Furthermore, exposure to airborne irritants from solvents or cleaning agents may induce respiratory diseases.[8,9] Increase in non-specific bronchial responsiveness can occur after acute massive exposure to gaseous pollutants.[10] Also, for indoor environments, access of fresh air is limited and the concentration of hazardous aerosol can be many times higher than outdoors.[11] Accordingly, controlling exposure to airborne pollutants in enclosed spaces is critical for the safety and health of individuals in a wide range of working environments.

Most working environments are operated with varying levels of control of environmental parameters, such as air mixing or ventilation rate.[12,13] Therefore, it is important to define what indoor environmental parameters affect exposure to airborne pollutants and determine how to reduce the exposure. Indoor airflow, including the airflow distribution in the vicinity of an occupant, is one of the important parameters affecting occupant exposure. An occupant's thermal plume, which is a warm, rising buoyant airflow caused by the temperature gradient between the human body and ambient air, can transport a pollutant around the body toward the breathing zone.[14]

Even in a room with mechanical ventilation, some degree of non-uniformity is present around an occupant.[15,16] Due to this non-uniform airflow around a human body, the actual pollutant concentration inhaled by an occupant can be significantly different from the ambient room concentration.[14,17,18] Source location with respect to an occupant is another important factor for inhalation exposure.[19] In general, different pollutant sources exist in different working environments, and many pollutants have distinct source locations. An important observation, to date, is that the concentration measured with a personal exposure monitor, especially for particulate pollutants, can be significantly higher than an indoor stationary monitor.[20–22] This phenomenon is known as the *personal cloud effect*.

The present study complements the previously mentioned studies on inhalation exposure and further explores the impact of the pollutant source location in the vicinity of the body on the concentration of inhaled air. This study investigates

**FIGURE 1.** Schematic diagram of the research procedure.
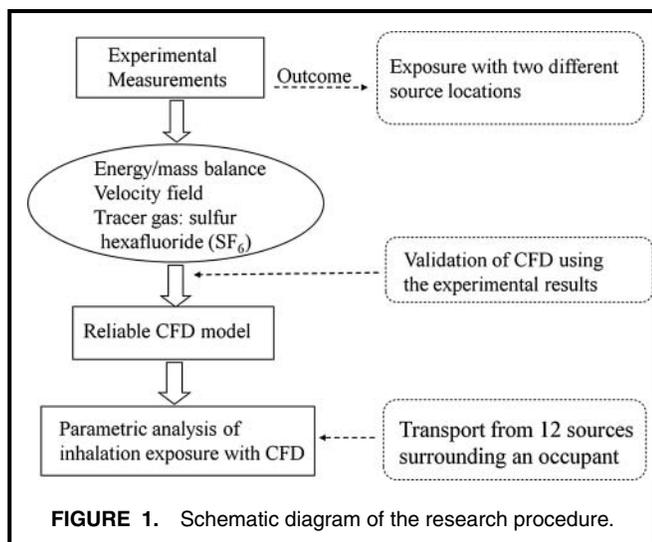
human exposure considering indoor air mixing and source locations with respect to a body and evaluates the contribution of each parameter to inhalation exposure. Results from this study can provide the research and engineering community with fundamental knowledge of pollutant distribution around the human body, which can be further used for analyses and control of personal exposure in working environments.

## METHODS

Experimental measurements and computational fluid dynamics (CFD) simulations were used to investigate breathing air quality in a room. Experimental measurements have the advantage of measuring first-hand data, but measurements often require high labor/equipment costs and often provide results for only several discreet points. Moreover, it is sometimes difficult to secure repeated measurements. On the other hand, CFD simulation is often less expensive and more informative. Using CFD necessitates addressing the uncertainties and errors associated with the CFD boundary conditions and numerical schemes.

As there are advantages and disadvantages of experimental measurement and CFD modeling,[23] this study combined the two methods to improve the quality of data. Experiments measured actual pollutant concentrations within a controlled experimental setup. Using the test results, the CFD model was validated. Then, the validated simulation models were used to predict airflow and pollutant dispersion in indoor environments where repetition of measurements was difficult. Figure 1 shows

the methodology diagram that describes the combination of experiments with CFD modeling.

Full-scale experiments were conducted to obtain experimental data for validation of the computational model. A thermal manikin in an environmental chamber was used to simulate an occupant in a realistic indoor environment. During the experiments, airflow velocity and tracer gas concentrations were monitored with the source at two different positions. The measurement apparatus is summarized in Table I.

The results provided benchmark data on pollutant transport that were required to develop a reliable CFD model. To ensure the quality of the CFD simulation results, air velocity, temperature, and pollutant concentrations resulting from the CFD simulation were compared with those measured in the experiments. In addition, based on suggestions in the literature,[24,25] the CFD parameters, including grid resolution and boundary conditions, were optimized for modeling room airflow distribution with various air mixing intensity (see the next section).

The developed CFD models were further used to conduct parametric analyses that determined the influences of source location and air mixing on the inhaled concentration. Parametric analyses were conducted to study pollutant dispersion from 12 different source locations in the vicinity of a human body. Finally, the contributions of these 12 source locations were quantified, using a parameter named "source accessibility." This parameter, which describes how easily a contaminant reaches the breathing zone, was used to evaluate the impact of each source location on the pollutant concentration in the inhaled air.

### Experimental Measurements and Validation of CFD Model

The experimental setup, as shown in Figure 2, was developed to investigate local airflow and pollutant transport in the vicinity of a thermal manikin. The setup included a 4.5 m × 5.5 m × 2.7 m full-scale environmental chamber equipped with an air handling unit (AHU), a thermal manikin, and sampling and measurement apparatus. The AHU was used to control the supply airflow rate and temperature in the room. The breathing thermal manikin was constructed to simulate human skin temperature and breathing. In the experiments, the total heat flux emitting across the skin surface was adjusted to 90 watts (W). The height and surface area of the seated manikin were 1.2 m and 1.3 m$^2$, respectively. The surface temperature ranged from 26°C to 29°C across the entire body. The tight-fitting clothes of the manikin provided an overall

**TABLE I.    Sampling Devices Used in the Validation Experiments**

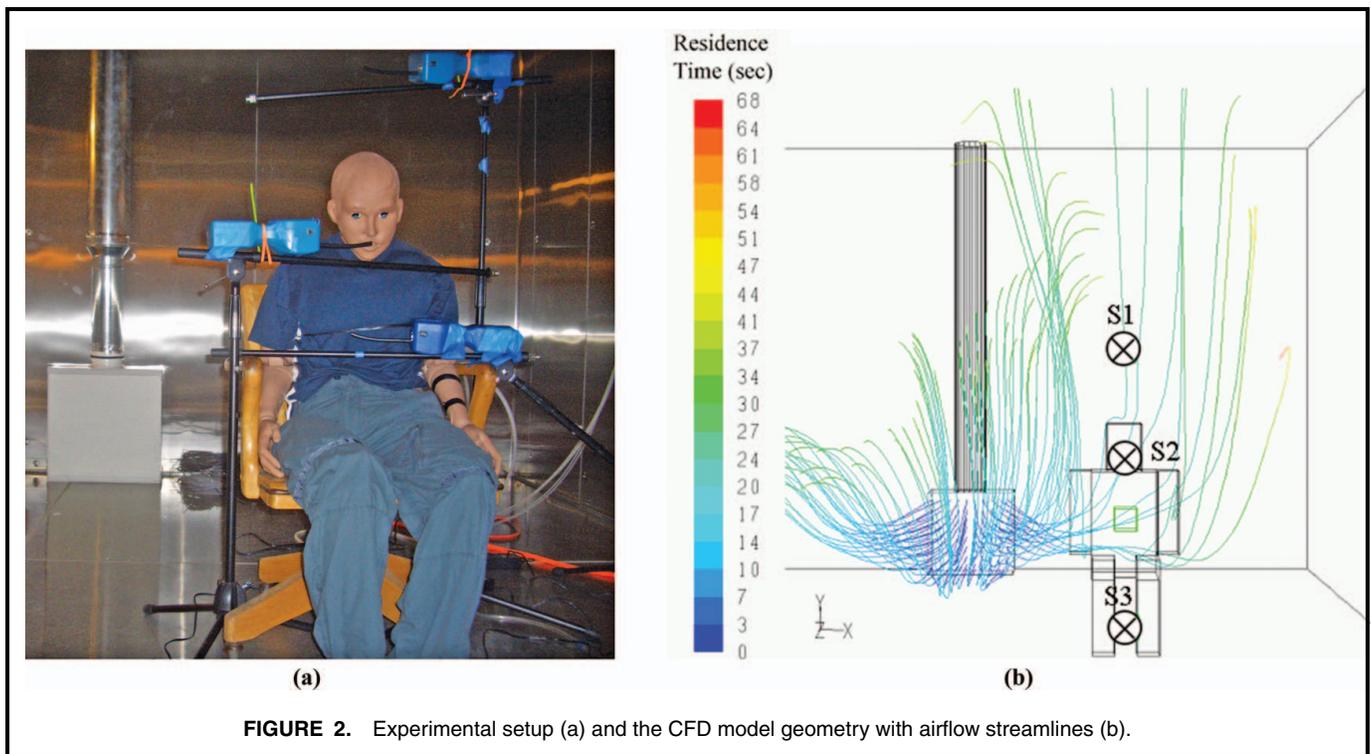| Measurement | Technology/Instrument | Range/Accuracy | Logging Interval |
|---|---|---|---|
| Air velocity | Hot-wire Anemometer (Sensor HT400) | 2.0–0.005 m/s (± 0.005 m/s) | 0.1 sec |
| Tracer gas (SF$_6$) | Gas Chromatographer, EDC (Lagus A.T. Inc., Model 101) | 1000–0.05 ppb–linear (± 2% of measured v.) | 2 min / 2 min |
| Temperature | Thermistors (Omega, 44000 Series) | 0–70°C (± 0.1°C) | 30 sec |

**FIGURE 2.** Experimental setup (a) and the CFD model geometry with airflow streamlines (b).

clothing insulation value of 0.5 clo. The manikin's breathing system provided realistic breathing airflow that consisted of a consecutive 2-sec inhalation and exhalation through the nose, with a short pause between them (0.5 sec).

The measurement apparatus monitored air velocity and temperature in addition to tracer gas concentrations (Table I). Velocity sensors recorded air speed and disturbances in the airflow due to turbulent fluctuations. With regard to the monitoring of tracer gas, two GC/ECD units (model 101 and AUTOTRAC; Lagus Applied Technology Inc., Escondido, Calif.) enabled monitoring of $SF_6$ concentrations every 2-min interval. The two analyzers were calibrated at the beginning of each experiment using an autocalibration system that employs a built-in calibration cylinder with known concentration of $SF_6$. In addition, readings from the two analyzers were compared and verified with simultaneous measurements of concentrations premixed in a Tedlar bag.

Experiments were conducted to validate CFD model predictions of the effect of source location with respect to an occupant on the pollutant concentration in the breathing zone. Experimental details are described in the article by Rim and Novoselac,[14] whose study previously developed a set of pollutant dynamics tests in the vicinity of a thermal manikin. The environmental chamber was furnished with indoor heat sources and objects that obstructed the airflow. This configuration was designed to develop a challenging case for CFD modeling of stratified air distribution and non-uniform pollutant distribution in a room. In the chamber, relatively cold (17°C) supply air at floor level was raised due to the heat dissipated from the manikin and heat source. During the experiments, the convective thermal plume was the dominant airflow in the vicinity of the manikin's body.

To simulate a pollutant, a tracer gas (0.1% $SF_6$) was injected at a flow rate of 20 mL/min at two source locations: (1) source position 1(P1), 1.5 m in front of the manikin's face; and (2) source position 2 (P2), 0.5 m behind the manikin at floor level. Tracer gas concentrations were analyzed at three monitoring positions in the vicinity of the manikin (Figure 2). Sampling position 1 (S1) was 0.25 m above the manikin's head. Sampling position 2 (S2) was in front of its mouth at a distance of 0.05 m. This position is intended to measure representative breathing air quality.[26] Sampling position 3 (S3) was 0.2 m above the floor, between the legs. At every sampling point, air samples were simultaneously collected for 1 hr and then analyzed using GC/ECD. Measurement data from the experiments provided information on the spatial pollutant distribution around the body and the level of inhalation exposure corresponding to a given source location.

The study established a numerical (CFD) model that accurately predicts the spatial and temporal transient pollutant distribution in the room and in the vicinity of the manikin (Figure 2b). CFD software FLUENT 6.3.26 (ANSYS, Inc., Lebanon, N.H.) was used for the numerical analyses of pollutant transport. Reynolds Averaged Navier-Stokes (RANS) equations were solved to predict airflow and pollutant transport in the vicinity of the manikin.

Significant efforts were dedicated to the verification of the developed CFD models and to ensure the quality of the simulation results with a relatively simple rectangular geometry of an

occupant (Figure 2). In the CFD simulation, volume-averaged concentrations for a 1 L sampling volume at three monitoring locations (feet, mouth, and above head) were calculated. Based on the comparison between measurements and CFD results, the CFD parameters, including the grid resolution and boundary conditions, were correspondingly adjusted.

Unstructured hexahedral grids were used. The finest grid was applied to the manikin surface, while the coarser grid was used for the rest of the space volume. Grid sensitivity was verified by refining the grid primarily in the vicinity of the occupant (seated thermal manikin). For the grid sensitivity analysis, thickness of the smallest cell adjacent to the manikin surface was altered from 10 mm to 1 mm. The cell size of 2 mm was found to produce a grid-independent solution considering the velocity and concentration distribution in the vicinity of the thermal manikin. For three cell sizes (2 mm, 6 mm, 10 mm), the uncertainty of discretization was calculated using the grid convergence index (GCI).[27]

$$GCI^{21} = \frac{1.25}{(r_{21})^p - 1} \left| \frac{f_1 - f_2}{f_1} \right| \qquad \textbf{(1)}$$

where $f_1$ is the quantity of interest on the finest grid, $f_2$ is the quantity of interest on the next-finest grid, $r_{21}$ is the grid refinement factor (the ratio of cell size between the two grids), and $p$ is the order of accuracy of the method.

In this study, the quantity of interest ($f$) was the average velocity magnitude for the 8 L sampling volume located 20 cm above the head (m/s), which is the most representative parameter for intensity of thermal plume. Using this velocity magnitude, the accuracy of model prediction for the natural convection flow around the body was determined. For the three grid numbers tested in our study, the order of accuracy ($p$) was calculated as 1.57. Detailed equations for calculating $p$ can be found in Celtik et al.[27] Table II shows the calculated GCI for the three selected grid resolutions. The numerical uncertainty in the fine-grid solution for the thermal plume goes down from 15% to 2.4% as refining the grid around the body; is refined further.

The experimental measurements indicated that the turbulence intensity above the head of a seated person approaches approximately 35%.[14] The turbulent airflow was simulated using the renormalization group (RNG) $k$-$\varepsilon$ model, given its better performance compared with the standard $k$-$\varepsilon$ model at relatively low computational cost.[28,29] However, one should be cautious when analyzing the results because RNG $k$-$\varepsilon$ model may under predict the extent of flow separation in low-velocity airflow.[29] Along with the turbulence model, standard wall functions were used to simulate the free-convection boundary layer. Airflow within the thermal boundary layer was considered fully turbulent. For the case of 110,000 cells, the value of y+ ranged from 12.0 to 28.0, which is desirable for applying wall functions with the RNG $k$-$\varepsilon$ model. Under these conditions, the CFD model calculated the temperature field with an accuracy of 0.5°C and generally predicts the velocity field within the experimental accuracy of 0.05 m/s.

A uniform velocity of 0.20 m/s at 17°C was applied at the inlet opening (0.26 m²), along with turbulence intensity of 10%. The surface area of the exhaust was 0.031 m², and a zero normal pressure gradient was applied to the exhaust. The thermal plume from the manikin was simulated using a convective heat flux as a thermal boundary condition. Based on the measurements of temperature at the chamber wall surfaces and the manikin surface, the convective and radiative portions of the total heat flux (90W) at manikin surface were calculated.

The convective portion (40W) of heat flux was distributed equally along the thermal manikin surface (Neumann boundary conditions), which generated buoyancy-driven flow and a realistic surface boundary layer across the manikin surface.[29] The radiative heat portion (the remaining heat flux 50W) from the thermal manikin is distributed along the chamber surfaces (using Neumann boundary conditions), and this enabled the energy balance in the room. Air temperature in the room was thermally stratified in the vertical direction due to the cold supply air at floor level, with low momentum and the heat release from the manikin and walls. In the numerical model, the Boussinesq approximation was enabled to capture the effects of variation in air density on the airflow in the vicinity of occupants and in the entire space. A reference temperature of 18°C is used.

### Parametric Analysis

The validated CFD model was further applied to produce data to analyze human exposure depending on air mixing and source location in the vicinity of an occupant. The CFD simulations evaluated the contribution of source locations to the concentration of inhaled air. Pollutant transport from the 12 sources in the vicinity of the manikin was simulated, as shown in Figure 3. For each of the 12 sources, the average concentration of the 1 L sampling volume in front of the

**TABLE II. Calculation of Grid Convergence Index (GCI) as an Uncertainty Estimate of the Fine-Solution Grid**

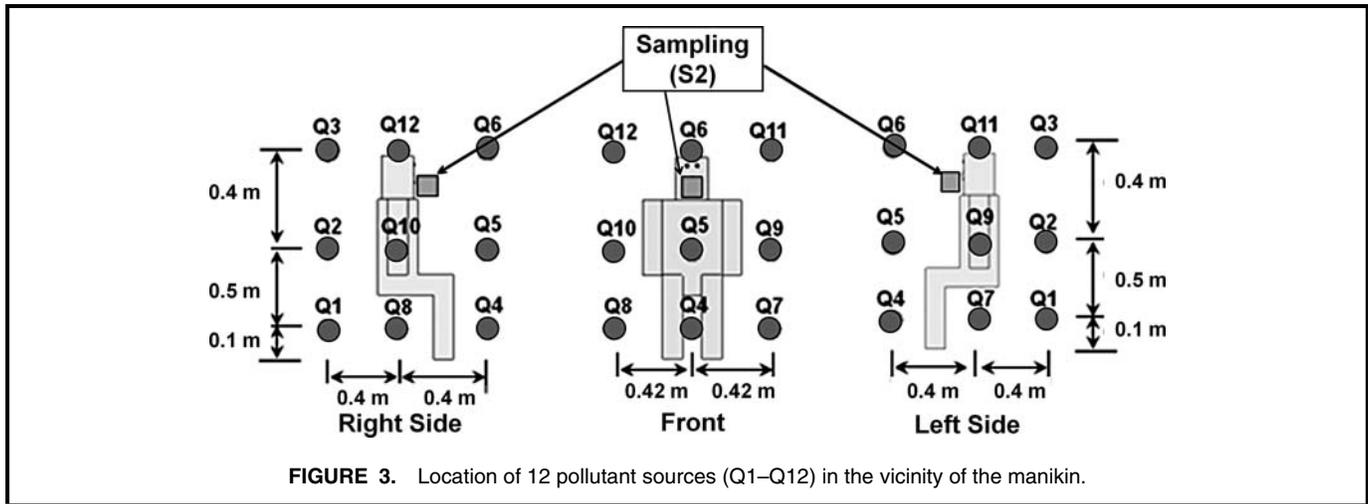| Number of Cells | $N_1 = 110{,}000$ | $N_2 = 80{,}000$ | $N_3 = 60{,}000$ |
|---|---|---|---|
| Smallest grid size (mm) | $h_1 = 2$ | $h_2 = 6$ | $h_3 = 10$ |
| Grid refinement factor | | $r_{21} = h_2/h_1 = 3$ | $r_{32} = h_3/h_2 = 1.67$ |
| Avg. velocity magnitude for the 8 L volume located 20 cm above the head (m/s) | $f_1 = 0.176$ | $f_2 = 0.160$ | $f_3 = 0.136$ |
| Grid convergence index | | $GCI^{21,\text{fine}} = 2.4\%$ | $GCI^{32,\text{fine}} = 15\%$ |

**FIGURE 3.** Location of 12 pollutant sources (Q1–Q12) in the vicinity of the manikin.

mouth was calculated. The source was active for 1 hr, and the time-integrated concentration in the breathing zone was calculated for this period. The calculated breathing concentration for each source location represents the contribution of source location to inhalation exposure.

To quantify the contribution of the source location to inhalation exposure, a parameter named source accessibility (SA) was calculated:[30]

$$SA(\tau) = \frac{\int_0^\tau C_{mouth}(\tau)d\tau}{C_{avg}\tau} \qquad \textbf{(2)}$$

where $SA(\tau)=$ source accessibility at time $\tau$, $C_{mouth}(\tau) =$ sampled concentration in front of the mouth at time $\tau$, $C_{avg} =$ average room concentration assuming steady-state source emission.

Source accessibility is a function of time and is associated with the ratio of breathing concentration to perfect mixing concentration. If the value is unity at a given time, the breathing zone concentration is the same as the uniform mixing concentration. Therefore, source accessibility represents the contribution of the given source to the breathing zone concentration and describes how easily a contaminant reaches the breathing zone relative to the room exhaust.[30,31]

In this study, source accessibility was averaged for 1 hr. During this period, a steady pollutant release from each source occurred. Each of the 12 sources was simultaneously released under the same airflow conditions. The time-averaged source accessibility was evaluated under three mixing conditions: low, medium, and high mixing intensities. These three mixing intensities were selected to simulate variation of air mixing occurring in several typical indoor working environments. For the three mixing intensities, three velocity momentum sources characterized by momentum forces of 0 Newton (N), 0.3 N, and 0.5 N were applied to 0.8 m³ air volume in the room. Note that units of Newton (N) are used here to quantify the velocity momentum sources in the space, as 1 N is the force needed to accelerate a mass of 1 kilogram of air at the rate of 1 meter per second per second. The momentum sources were located approximately 2 m away from the manikin and 0.2 m away from the chamber wall.

Table III summarizes the average air speed for the whole room and near the manikin for the three mixing intensities. Data in Table III indicate that the average room air speed increases with an increase in mixing intensity, whereas the air speed near the manikin surface does not vary much across the three mixing conditions, which is likely due to the presence of the thermal plume around the manikin's body.[16,32] Source accessibility distribution in relation to the air mixing intensity reveals the intensity of the thermal plume depending on air mixing and resulting pollutant concentration in the breathing zone.

## RESULTS

This section discusses the results of CFD validations, followed by the major study results from the parametric analysis of source accessibility with 12 source locations.

### Results of CFD Validation: Pollutant Distribution in the Vicinity of the Manikin

Figure 4 shows a comparison of measured and simulated steady-state concentration distributions of the tracer gas in the vicinity of the body for the two source positions studied: P1 (1.5 m in front of the face) and P2 (0.5 m behind the

**TABLE III. Average Air Speed for the Whole Room and for the First Cells Adjacent to Manikin Surface**

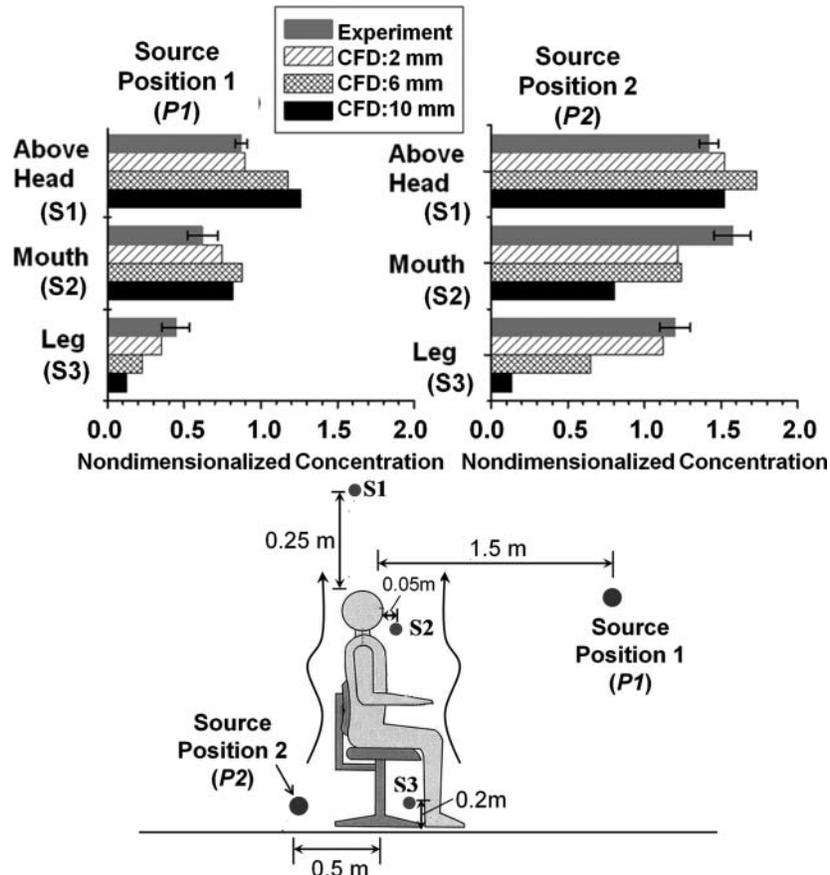| Mixing Intensity | Average Room Air Speed (m/s) | Average Air Speed of the First Cell Near Manikin Surface (m/s) |
|---|---|---|
| Low (0N) | 0.036 | 0.092 |
| Medium (0.3N) | 0.084 | 0.088 |
| High (0.5N) | 0.11 | 0.087 |

**FIGURE 4.** Tracer gas concentrations at three monitoring points (S1, S2, and S3) for two different sources (P1 and P2). Experiment vs. CFD simulations (CFD simulation results are with the three different grid thicknesses (2 mm, 6 mm, and 10 mm) for the smallest cell adjacent to the manikin surface. All concentrations are normalized by the concentration at the exhaust.

leg at the floor level). When the source was at P1, the pollutant was moved toward the manikin's face by the overall airflow. With the source at P2, the pollutant was transported into the breathing zone of the manikin by the occupant's thermal plume. Simulation results of pollutant dispersion from the two source positions were compared using a normalized concentration.

Results in Figure 4 show the general pattern of concentration distribution in the vicinity of the manikin for the three different grid thicknesses (2 mm, 6 mm, and 10 mm) for the smallest cell adjacent to the manikin surface. Finer grid resolution produces better agreement, even though the simulation results do not perfectly match the experimental results. The largest discrepancy (up to 25%) between the experiment and CFD was observed in the region close to the mouth, which may be explained by the simplified manikin geometry or absence of respiration in the CFD simulation.[26,33] Also, the steep gradient of airflow velocity and pollutant concentration around the thermal plume might cause the errors. However, the similar trend in the concentration distribution between measurements and CFD suggests that the applied CFD model can provide insight into pollutant distribution in the vicinity of the body with different source locations.
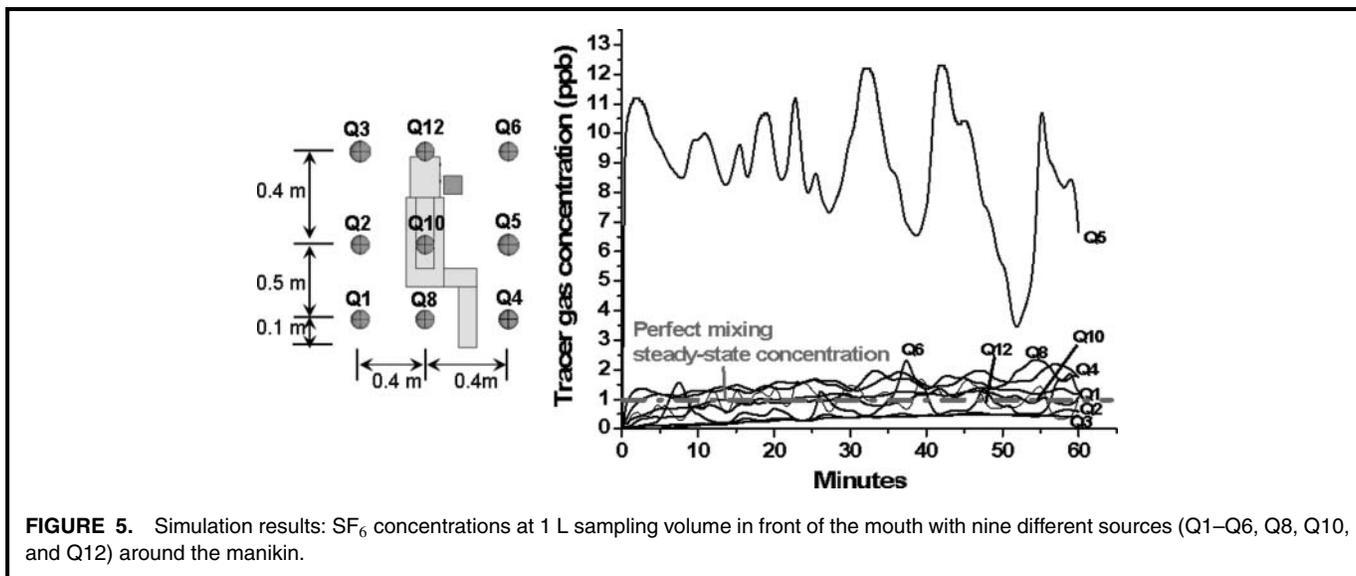
## Impact of Source Location and Airflow Mixing on Exposure

This section presents the major results from the parametric analysis, including (1) effects of source location on breathing zone concentration, and (2) source accessibility distribution associated with air mixing intensity.

### Effect of Source Location on Exposure: Source Accessibility Distribution

The impact of source location on the breathing zone concentration is described in Figure 5, which shows the part of the simulation results from the source location analysis, along with tracer gas concentration profiles in the breathing zone for nine different sources in the vicinity of the manikin. Figure 5 shows that pollutant dispersion from a source to the breathing zone varies with source location. Overall, breathing concentrations due to the sources in the vicinity of the manikin are comparable to or higher than perfect-mixing concentration. This finding is in general agreement with the previous study,[22,34] which observed high breathing concentration when the contaminant source is in near proximity to the occupant.

Figure 6 illustrates source accessibility distribution for the 12 different pollutant locations in the vicinity of the body,

**FIGURE 5.** Simulation results: $SF_6$ concentrations at 1 L sampling volume in front of the mouth with nine different sources (Q1–Q6, Q8, Q10, and Q12) around the manikin.

which is the result with low air mixing intensity (0 N in Table III). The numbers above the sources indicate time-averaged accessibility of the source to the breathing zone over 1 hr. (Eq. 2). In other words, the numbers represent the contribution of the given source to the breathing zone concentration during the source emission period of 1 hr. If the value is equal to 1.0, breathing zone concentration is equal to the concentration under uniform air mixing. If the value is larger than 1.0, breathing zone concentration for the source would be larger than the concentration calculated with uniform mixing assumption. In this way, source accessibility quantifies how different locations affect exposure for a considered pollutant source location and airflow distribution.

According to Figure 6, source accessibility is the highest for the source in the chest region (approximately nine times larger than perfect mixing), while the source accessibility is the lowest for the sources in the back and head regions. In

general, the source accessibility is larger with the sources close to the floor than the sources at head level. This trend is in agreement with the study by Kim et al.,[35] which reported the higher contribution of a floor source to the breathing zone concentration of a standing person compared with the sources at ceiling and sidewalls.

### Source Accessibility Distribution Associated with Air Mixing Intensity

Overall, results from the parametric analysis provide information about the influence of air mixing on the source accessibility distribution. Time-averaged source accessibility distributions for low, medium, and high mixing are summarized in Table IV. The source accessibility observed with the low mixing intensity varies with source location more so than those observed with high mixing intensity. In the cases with low and medium mixing intensity, source accessibility is the
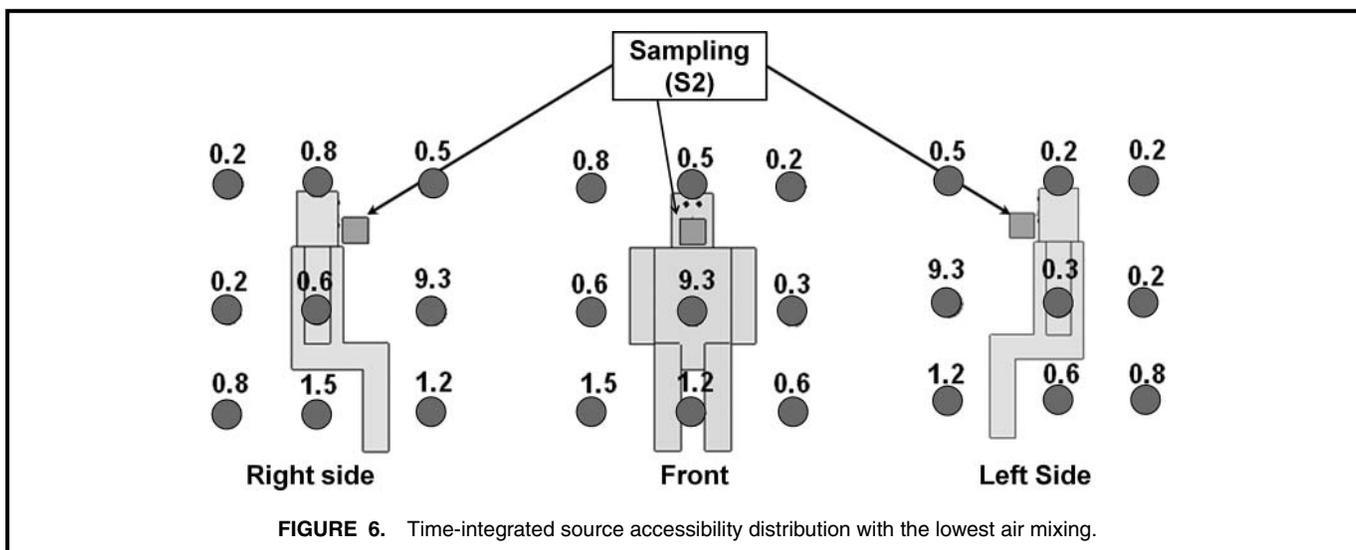


**FIGURE 6.** Time-integrated source accessibility distribution with the lowest air mixing.

**TABLE IV.   Source Accessibility Distribution for 12 Pollutant Sources (Q1–Q12 Shown in Figure 3) Associated with Varying Levels of Mixing Intensity**

| Mixing Intensity | Time-Averaged Source Accessibility | | | | | | | | | | | |
|---|---|---|---|---|---|---|---|---|---|---|---|---|
| | Q1 | Q2 | Q3 | Q4 | Q5 | Q6 | Q7 | Q8 | Q9 | Q10 | Q11 | Q12 |
| Low | 0.80 | 0.22 | 0.17 | 1.2 | 9.3 | 0.53 | 0.58 | 1.3 | 0.32 | 0.63 | 0.18 | 0.80 |
| Medium | 1.1 | 0.70 | 0.34 | 0.67 | 3.6 | 0.10 | 0.47 | 0.66 | 0.33 | 1.49 | 0.29 | 0.38 |
| High | 0.91 | 0.53 | 0.09 | 0.17 | 0.71 | 1.1 | 0.33 | 0.10 | 0.86 | 0.11 | 0.16 | 0.07 |

highest at Q5 (the source in the front chest region). Under low and medium mixing conditions, breathing zone concentration due to the source at Q5 (Figure 3) is approximately nine times and four times greater than uniform mixing concentration, respectively; however, under the high mixing condition, source accessibilities are relatively uniform. This result indicates that with large room air mixing, the breathing concentration has small dependence on source location.

## DISCUSSION

Among all the analyzed source locations, the location in the chest region (Q5) had the highest contribution to the breathing concentration. This pattern may be explained by the airflow distribution in the vicinity of the manikin. Figure 7 illustrates the airflow pattern around the simulated occupant. A buoyancy-driven thermal plume develops in the vicinity of the body because of the temperature gradient between the body surface and ambient air. In this case, the plume transports the pollutants upward to the breathing region and above the head. This upward thermal plume seems to cause significant contaminant transport from Q5 (chest region) toward the breathing zone. These findings complement previous studies[34,35] that found high levels of exposure to the sources above the hip level of a standing person.

It seems plausible that the buoyancy-driven thermal plume transports the pollutant from a lower zone to the upper breathing zone, and the effect of the thermal plume on the breathing concentration is the largest with the source in the front chest region. It is also likely that the thermal plume moves sources in the head region away from the breathing zone. These findings have implications for exposure analysis of workers who work with sources in the front chest region. When control of source strength is difficult, moving the source location farther away from the chest or reducing the intensity of the buoyant airflow around the body can be a possible solution for controlling the exposure to airborne pollutants close to the body.

It has also been found that the concentration distribution in the space tends to be uniform in the vicinity of the body as air mixing increases with occupant activity.[19] The present study showed that the air mixing condition is associated with potential variability of exposure for a contaminant release. The study results suggest that the breathing zone concentration is potentially high with little air mixing in a space, while an increase in air mixing can mitigate unfavorable dispersion of a pollutant emitted in the occupant's vicinity. With little air
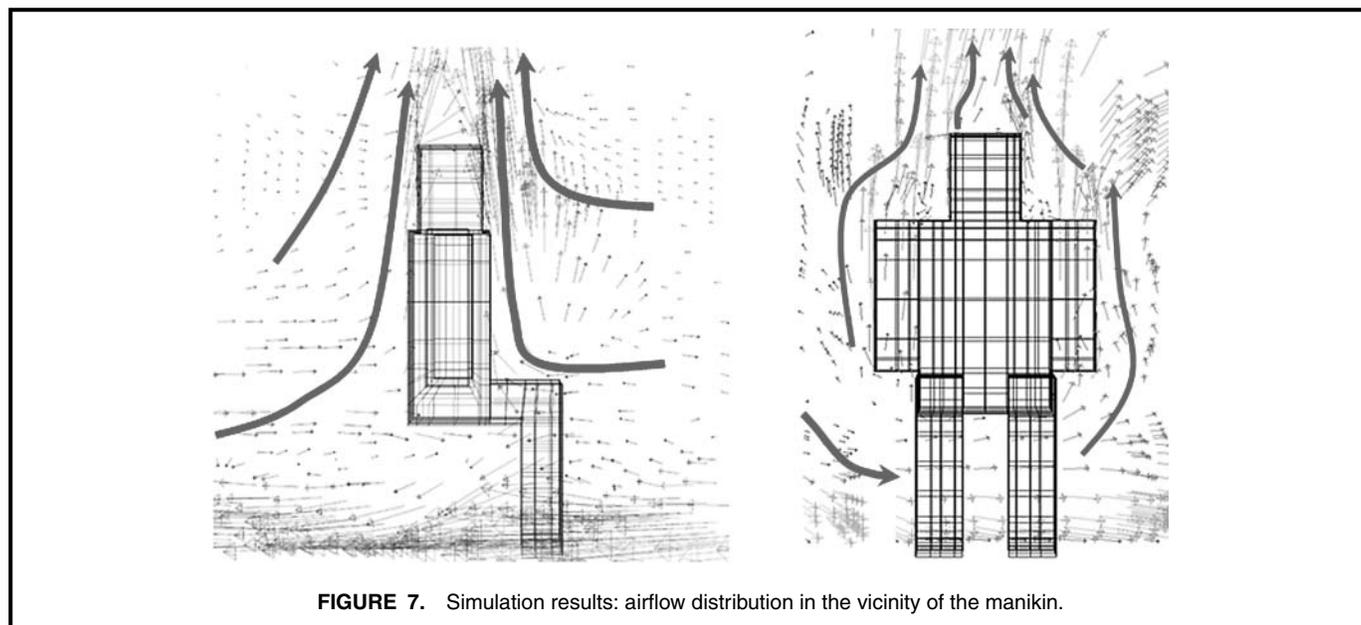


**FIGURE 7.**   Simulation results: airflow distribution in the vicinity of the manikin.

mixing, buoyancy generated near the human body seems to increase the impact of the thermal plume, while increased air mixing causes disruption of the thermal plume. Accordingly, in the absence of room air mixing, the thermal plume seems to have a great influence on exposure, whereas with increased air mixing, the impacts of the thermal plume and source locations on occupant exposure become less important.

## CONCLUSIONS

Using experimentally validated CFD simulations, this study investigated occupational exposure as a function of source location with respect to a human body. The study found that a high acute exposure to airborne pollutants may occur when little air mixing exists in a space. In addition, the results indicate that for estimation of exposure, it may not be appropriate to assume perfect air and pollutant mixing in the space. When little air mixing exists around the body, the pollutant concentration in a person's front chest region had the largest influence on the breathing zone concentration. This is due to the buoyancy-driven thermal plume that transports the pollutant from the chest region to the upper breathing zone. However, the impacts of the thermal plume on an occupant's exposure seem to be less important as room air mixing increases. Overall, the study results provide a basis for the relationship between source location and breathing zone concentrations relative to the normal background concentrations for the two most fundamental airflow distribution environments: (1) buoyancy-driven flow, and (2) high air mixing. The study results can be used to estimate occupational exposure with similar airflow patterns at various workplaces.

## ACKNOWLEDGMENTS

## REFERENCES

1. **Fisk, W.J., and A.H. Rosenfeld:** Estimates of improved productivity and health from better indoor environments. *Indoor Air 7*:158–172 (1997).
2. **Mendell, M.J., Fisk, W.J. Kreiss, et al.:** Improving the health of workers in indoor environments: Priority research needs for a national occupational research agenda. *Am. J Pub. Health 92*:1430–1440 (2002).
3. **Duarte-Davidson R., C. Courage, L. Rushton, and L. Levy:** Benzene in the environment: An assessment of the potential risks to the health of the population. *Occup. Environ. Med. 58(1)*:2–13 (2001).
4. **Matheson M., G. Benke, J. Raven, et al.:** Biological dust exposure in the workplace is a risk factor for chronic obstructive pulmonary disease. *Thorax 60(8)*:645–651 (2005).
5. **Randem, B., B. Ulvestad, I. Burstyn, et al.:** Respiratory symptoms and airflow limitation in asphalt workers. *Occup. Environ. Med. 61(4)*:367–369 (2004).
6. **Delfino, R.:** Epidemiologic evidence for asthma and exposure to air toxics: Linkages between occupational, indoor, and community air pollution research. *Environ. Health Perspect. 110*:573–589 (2002).
7. **Balmes, J., M. Becklake, P. Blanc, et al.:** American Thoracic Society statement: Occupational contribution to the burden of airway disease. *Am. J. Resp. Crit. Care Med. 167*:787–797 (2003).
8. **Nijem, K., P. Kristensen, A. Al-Khatib, et al.:** Prevalence of neuropsychiatric and mucous membrane irritation complaints among Palestinian shoe factory workers exposed to organic solvents and plastic compounds. *Am. J. Ind. Med. 40(2)*:192–198 (2001).
9. **Wolkoff, P., T. Schneider, J. Kildeso, et al.:** Risk in cleaning: Chemical and physical exposure. *Sc. Tot. Environ. 215(1–2)*:135–156 (1998).
10. **Boulet, L.P.:** Increases in airway responsiveness following acute exposure to respiratory irritants. Reactive airway dysfunction syndrome or occupational asthma? *Chest 94(3)*:476–481 (1998).
11. **Ozkaynak, H., J. Xue, J. Spengler, et al.:** Personal exposure to airborne particles and metals: Results from the particle team study in Riverside, California. *J. Expo. Anal. Environ. Epidemiol. 6(1)*:57–78 (1996).
12. **Drescher, A.C., C. Lobascio, A.J. Gadgil, et al.:** Mixing of a point-source indoor pollutant by forced convection. *Indoor Air 5(3)*:204–214 (1995).
13. **Seppanen, O.A., W.J. Fisk, and M.J. Mendell:** Association of ventilation rates and $CO_2$ concentrations with health and other responses in commercial and institutional buildings. *Indoor Air 9*:226–52 (1999).
14. **Rim, D., and A. Novoselac:** Transport of particulate and gaseous pollutants in the vicinity of a human body. *Build. Environ. 44(9)*:1840–1849 (2009).
15. **Johnson, A.. and B. Fletcher, and C. Saunders:** Air movement around a worker in a low-speed flow field. *Ann. Occup. Hyg. 40(1)*:57–64 (1996).
16. **Gao, N.P., and H.L. Niu:** CFD study of the thermal environment around a human body: A review. *Indoor Built Environ. 14(1)*:5–16 (2005).
17. **Rim, D., A. Novoselac, and G. Morrison:** The influence of chemical interactions at the human surface on breathing-zone levels of reactants and products. *Indoor Air 19*:324–334 (2009).
18. **Ferro, A.R., R.J. Kopperud, and L. Hildemann:** Elevated personal exposure to particulate matter from human activities in a residence. *J. Expo. Analysis Environ. Epidemiol. 14*:S34–S40 (2004).
19. **Brohus, H., and P.V. Nielsen:** Personal exposure in displacement ventilated rooms. *Indoor Air 6(3)*:157–167 (1996).
20. **Rabinovitch, N., A.H. Liu, L.N. Zhang, et al.:** Importance of the personal endotoxin cloud in school-age children with asthma. *J. Allergy Clin. Immunol. 116(5)*:1053–1057 (2005).
21. **Rodes, C., P.A. Lawless, G.F. Evans, et al.:** The relationships between personal PM exposures for elderly populations and indoor and outdoor concentrations for three retirement center scenarios. *J. Expo. Anal. Environ. Epidemiol. 11(2)*:103–115 (2001).
22. **McBride, S.J., A.R. Ferro, W.R. Ott, et al.:** Investigations of the proximity effect for pollutants in the indoor environment. *J. Expo. Anal. Environ. Epidemiol. 9(6)*:602–621 (1999).
23. **Chen, Q.:** Ventilation performance prediction for buildings: A method overview and recent applications. *Building and Environment. 44*: 848–858 (2009).
24. **Sørensen, D.N., and P.V. Neilsen:** Quality control of computational fluid dynamics in indoor environments. *Indoor Air 13(1)*:2–17 (2003).
25. **Chen, Q., and J. Srebric:** A procedure for verification, validation, and reporting of indoor environment CFD analyses. *Int. J. HVAC Res. 8*:201–216 (2002).
26. **Melikov, A., and J. Kaczmarczyk:** Influence of geometry of thermal manikins on concentration distribution and personal exposure. *Indoor Air 17(1)*:50–59 (2007).
27. **Celtik, I.B., U. Ghia, P.J. Roache, et al.:** Procedure for estimation and reporting of uncertainty due to discretization in CFD applications. *J. Fluid. Eng. 130*:078001 (2008).

28. **Chen, Q.:** Comparison of different k-$\varepsilon$ models for indoor air flow computations. *Num. Heat Trans. Part B 28(3)*:353–369 (1995).

29. **Craven, B.A., and G.S. Settles:** A computational and experimental investigation of the human thermal plume. *J. Fluid. Eng. 128*:1251–1258 (2006).

30. **Yang, J., X. Li, and B. Zhao:** Prediction of transient contaminant dispersion and ventilation performance using the concept of accessibility. *Energy Build. 36*:293–299 (2004).

31. **Li, X., and J. Chen:** Evolution of contaminant distribution at steady airflow field with and arbitrary initial condition in ventilated space. *Atmos. Environ. 42*:6775–6784 (2008).

32. **Murakami, S., S. Kato, and J. Zeng:** Combined simulation of airflow, radiation and moisture transport for heat release from a human body. *Build. Environ. 35(6)*:489–500 (2000).

33. **Topp, C., P.V. Nielsen, and D.N. Sørensen:** Application of computer simulated persons in indoor environmental modeling. *ASHRAE Trans. 108(2)*:1084–1089 (2002).

34. **Kulmala I., A. Saamanen, and S. Enbom:** The effect of contaminant source location on worker exposure in the near-wake region. *Ann. Occup. Hyg. 40(5)*:511–523 (1996).

35. **Kim T., and M.R. Flynn:** Airflow pattern around a worker in a uniform freestream. *Am. Ind. Hyg. Assoc. J. 52*:287–296 (1991).